Methods and Applications in Fluorescence

RECEIVED
13 November 2016

REVISED
23 February 2017

ACCEPTED FOR PUBLICATION
2 March 2017

PUBLISHED
29 March 2017

PAPER

Crosslinked polymer nanoparticles containing single conjugated polymer chains

Rodrigo A Ponzio[1,2,3,4], Yésica L Marcato[1], María L Gómez[1,3,4], Carolina V Waiman[1,3], Carlos A Chesta[1,3,4] and Rodrigo E Palacios[1,3,4]

[1] Departamento de Química, Facultad de Ciencias Exactas, Físicas y Naturales, Universidad Nacional de Río Cuarto, Córdoba, Argentina
[2] Departamento de Física, Facultad de Ciencias Exactas, Físicas y Naturales, Universidad Nacional de Río Cuarto, Córdoba, Argentina
[3] Consejo Nacional de Investigaciones Científicas y Técnicas (CONICET), Argentina
[4] Instituto de Investigaciones en Tecnologías Energéticas y Materiales Avanzados (IITEMA), Argentina

E-mail: rpalacios@exa.unrc.edu.ar

Keywords: conjugated polymer, crosslinked nanoparticles, hyperspectral fluorescence image analysis, Brownian motion single particle tracking, single particle fluorescence blinking

Supplementary material for this article is available online

Abstract

Conjugated polymer nanoparticles are widely used in fluorescent labeling and sensing, as they have mean radii between 5 and 100 nm, narrow size dispersion, high brightness, and are photochemically stable, allowing single particle detection with high spatial and temporal resolution. Highly crosslinked polymers formed by linking individual chains through covalent bonds yield high-strength rigid materials capable of withstanding dissolution by organic solvents. Hence, the combination of crosslinked polymers and conjugated polymers in a nanoparticulated material presents the possibility of interesting applications that require the combined properties of constituent polymers and nanosized dimension. In the present work, F8BT@pEGDMA nanoparticles composed of poly (ethylene glycol dimethacrylate) (pEGDMA; a crosslinked polymer) and containing the commercial conjugated polymer poly(9,9-dioctylfluorene-alt-benzothiadiazole) (F8BT) were synthesized and characterized. Microemulsion polymerization was applied to produce F8BT@pEDGMA particles with nanosized dimensions in a ~25% yield. Photophysical and size distribution properties of F8BT@pEDGMA nanoparticles were evaluated by various methods, in particular single particle fluorescence microscopy techniques. The results demonstrate that the crosslinking/polymerization process imparts structural rigidity to the F8BT@pEDGMA particles by providing resistance against dissolution/disintegration in organic solvents. The synthesized fluorescent crosslinked nanoparticles contain (for the most part) single F8BT chains and can be detected at the single particle level, using fluorescence microscopy, which bodes well for their potential application as molecularly imprinted polymer fluorescent nanosensors with high spatial and temporal resolution.

Introduction

Conjugated polymers (CP) are organic macromolecules formed by a series of repeating units (monomers) linked together by a succession of single and double (or triple) bonds alternated along the backbone chain. This structure gives the material unique properties such as high electrical conductivity, mechanical processability, and the ability to emit light in the visible region of the electromagnetic spectrum after optical or electrical excitation. Because of these properties, CP are used in various organic-electronic devices such as solar cells [1, 2], organic light emitting diodes (OLED) [3], sensors [4], etc. Recently, CP nanoparticles (CPNPs) were synthesized, which are useful for various applications [5–7]. In particular nanoparticles (NP) of the commercial conjugated polymer F8BT have been prepared with average radii between 5 and 30 nm and low size dispersion. These particles possess high brightness and photochemical stability, allowing their detection/monitoring at the individual-particle level with high spatial and temporal resolution [7, 8]. These characteristics make them particularly suitable for fluorescent labeling and/or sensing applications.

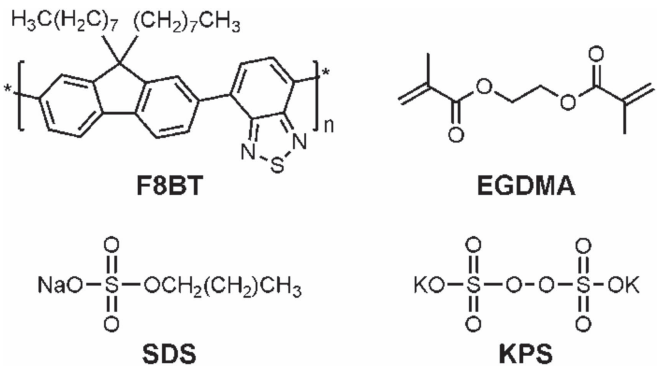

Scheme 1. F8BT, EGDMA, SDS, and KPS molecular structures.

Furthermore, molecular imprinting polymers (MIPs) are materials which exhibit high selectivity and affinity for a specific substrate through binding sites produced by self-assembly of a template molecule (analyte of interest) with monomers containing appropriate functional groups (which have strong monomer-template specific interactions), followed by crosslinked copolymerization [9, 10]. After polymerization, the template molecule is removed from the polymer, leaving recognition/binding sites which in terms of size, shape, and functional affinity are complementary to the template [11]. Crosslinking is essential to preserve the three-dimensional structure of recognition/binding sites upon template washing/removal. MIP generation using CP matrices, and particularly CPNPs, presents the possibility of various applications such as in ultra-sensitive analyte sensing technologies [12]. However, polymer chains in CPNPs are held together by van der Waals forces, and their structure is not rigid enough to withstand washing steps usually employed to remove occluded templates (within the polymer matrix) in the molecular imprinting process.

In the present work we prepared polymer NP formed by a rigid crosslinked poly-EGDMA (pEGDMA) matrix entrapping F8BT polymer chains (F8BT@pEGDMA NP). The particles were synthesized by microemulsion polymerization inside micelles containing F8BT chains and EGDMA crosslinker monomers. The particles were characterized by UV–visible absorption spectroscopy, atomic force microscopy (AFM), dynamic light scattering (DLS), Brownian motion single particle tracking (BM-SPT), spectral fluorescence microscopy, and monitoring of single particle fluorescence intensity transients. The synthesized particles have nanosized dimensions and are highly fluorescent. Moreover F8BT@pEGDMA NPs maintain their integrity in organic solvents such as toluene and ethyl acetate, suggesting that the three-dimensional pEGDMA matrix imparts sufficient rigidity to the particles to make them suitable for molecular imprinting. Finally, we demonstrate that these particles can be detected at the single particle level with high spatial and temporal resolution using fluorescence microscopy.

Experimental methods

Materials

Poly(9,9-dioctylfluorene-alt-benzothiadiazole) (F8BT; MW = 70 000 kg mol^{-1}, PDI = 2.4, American Dye Source Inc.), potassium persulfate (KPS; Sigma-Aldrich, >99%), sodium dodecyl sulfate (SDS; Sigma-Aldrich, >99%), ethyl acetate (EtOAc; Sigma-Aldrich, 99.7%), sulfuric acid (H_2SO_4; Cicarelli, 98%), hydrogen peroxide (H_2O_2; Cicarelli, 30% v/v), toluene (Sigma-Aldrich, 99%), acetone (Sintorgan, 99.5% HPLC grade), and methanol (MeOH; Merk, 99.8% HPLC grade) were used as received. Ethylene glycol dimethacrylate (EGDMA; Sigma-Aldrich, 99.8%) was used prior to elimination of polymerization inhibitors (hydroquinones) by repeated elution through a column loaded with Dehibit 200 (Polyscience) resin. Chemical structures of F8BT, EGDMA, SDS, and KPS are shown in scheme 1. Tetrahydrofuran (THF; HPLC grade, Cicarelli) was refluxed for 5 h with potassium hydroxide pellets (KOH; pro-analysis grade, Taurus) and subsequently distilled over freshly activated molecular sieves (4 Å, Aldrich). Double-distilled water was further purified by an ELGA PURELAB Classic UV system (~18.2 MΩ cm^{-1}) to remove ions, organic and particulate matter (0.2 μM filter). Nitrogen (N_2, 99.99%, Air Liquide) was used as received.

F8BT NP synthesis

F8BT NP were prepared by the re-precipitation method [5, 6]. F8BT was dissolved (with the aid of sonication and mild heating ~40 °C) in freshly distilled THF to a concentration of ~0.5 g L^{-1}. The solution was filtered with a 0.2 μm pore-size PTFE membrane syringe filter (Iso-Disc, Sigma-Aldrich) to remove any undissolved polymer. The concentration of the filtered solution was recalculated by comparing absorption spectra before and after filtration, and the resulting solution was diluted to a final concentration

of 0.1 g L^{-1}. 0.3 mL of this solution were quickly injected into 2.5 mL of water under vigorous stirring. Upon contact with water the polymer chains collapse forming NP containing of one or several chains (nano-aggregates) [5, 6].

F8BT@pEGDMA NP synthesis

The F8BT@pEGDMA NP were synthesized by micro-emulsion polymerization. 0.3 mL of F8BT (0.1 g L^{-1} and 0.13 mL of EGDMA (0.03 mol L^{-1}) solutions in THF were independently injected into 2.3 mL of water containing SDS (15 mmol L^{-1}) with continuous stirring. The resulting mixture was purged with N_2 for 10 min in a glycerin bath at 80 ± 0.1 °C (Memmert, WNB 7). After N_2 purging 100 μL of freshly prepared KPS water solution (0.14 mol L^{-1}) was injected in the pre-polymeric mixture and left to react for 20 h in the glycerin bath. KPS is a well know radical polymerization initiator that can be thermally activated [13]. EGDMA has been previously used as crosslinker to prepare polymer NP containing hydrophobic monomers (e.g. methyl methacrylate, butyl acrylate, and butyl methacrylate), by microemulsion polymerization in water using SDS as surfactant and KPS as initiator [14, 15]. Thus, despite EGDMA's moderate water solubility (~1 gr L^{-1}), it is reasonable to assume that both F8BT and EGDMA are at least partially distributed within or near the hydrophobic phase of the microemulsion. Our results indicate (*vide infra*) that upon polymerization these systems yield F8BT@pEGDMA NP where F8BT chain(s) are retained within the pEGDMA crosslinked matrix. After polymerization SDS was eliminated by three cycles of particle precipitation (centrifugation at 13 000 rpm for 1 h) and re-suspension in 2 mL of clean water. After each cycle, surfactant removal was tested by cooling the supernatant to 6 °C (SDS Kraft temperature [16]). No SDS precipitate was observed upon cooling the final centrifugation step supernatant. Analogous precipitation/re-suspension cycles were carried out using MeOH to remove EGDMA excess. The purified pellet was dried to constant weight at 40 °C and the synthesis yield was calculated as 25% for F8BT@pEGDMA NP. Particle suspensions in different solvents were prepared by sonication (5 min, Arcano, PS-30A) of particles in the desired solvent.

Atomic force microscopy (AFM)

Samples were prepared by spincasting NP suspensions (12 mg L^{-1}) on freshly cleaved mica substrates (SPI, Grade V-1 Muscovite). AFM images were obtained on an Agilent 5400 AFM microscope in tapping mode operating at a scan rate of 12.05 microns s^{-1}, with resolution of 512 × 512 pixels and a physical image size of 15 × 15 μm, using a cantilever (μMasch, NSC15/AIBS) with nominal frequency of vibration of 325 kHz, radius of curvature <10 nm, and force constant of 46 N m^{-1}. Images (five images per sample) were processed with the Gwyddion program [17]. Field curvature effects were first corrected using the 'Remove Polynomial Background', 'Correct lines by matching height median', and 'Level data by mean plane subtraction' functions. The resulting images were then analyzed, with the same program, to select particles using the 'Mark grains by threshold' function and finally the 'Grain Distributions' function was used to obtain the maximum height of each identified particle. The resulting data were used to build NP height histograms.

Dynamic light scattering (DLS)

Measurements were performed with a Zeta-Sizer Nano ZS90 Instrument, at a temperature of 25 °C. Light scattering results were analyzed with Zetasizer software (provided by the instrument manufacturer) to obtain hydrodynamic radius distributions by number. Particle suspensions for DLS were prepared with water filtered through 0.2 μm pore filters right before data acquisition. Extreme care was taken to reduce contamination by dust.

Fluorescence microscopy

Fluorescence microscopy single particle tracking (SPT) and topographic images were acquired with a home-built inverted epi-fluorescence microscope assembled on an anti-vibration optical table (Thorlabs, PTM11109). Excitation was provided by the 458 nm and 488 nm lines of a CW Ar-ion laser (Modu-Laser, Stellar Pro L 300), a linear polarizer (Thorlabs, LPVISE100-A), and a quarter waveplate (Thorlabs, AQWP05M-600) used to obtain a circularly polarized beam. The laser beam was later magnified 10 times using a pair of lenses (Thorlabs, LA1540-A-ML and Thorlabs, AC254-150-A-ML) and focused with a third lens (Thorlabs, LA1979-A) at the back focal plane of a Reichert 40 × 0.66 NA objective previous reflection on a dichroic mirror (Edmund #86-331 for 458 nm or Semrock DI01-R488-25x36 for 488 nm). Emission from the sample was collected through the same objective, spectrally filtered with a long pass filter (Semrock BLP01-458R-25 for 458 nm or Semrock BLP01-488R-25 for 488 nm), and focused with a tube lens (Nikon, ITL200 # Thorlabs) on the chip of an EM-CCD camera (Andor, iXonEM+897) to form fluorescence topographic images of the sample (x, y, I_f) where x and y coordinates correspond to sample spatial dimensions in the focal plane and the I_f coordinate corresponds to the emission intensity.

Acquisition of spectral information was achieved by redirecting (with a folding mirror) the microscope collection path and focusing it on the entrance slit of an imaging spectrograph (Andor, Shamrock 303i). In spectral mode a four-dimensional hyperspectral data cube (x, y, λ, I_f) was constructed where the λ coordinates correspond to emission spectral dimensions. The spectrograph is equipped with a high throughput

diffraction grating (50 grooves mm^{-1}, blazed at 600 nm), an EM-CCD camera coupled to the exit slit, and a variable aperture motorized entrance slit. Data were acquired in spatial scanning mode where emission from a narrow line (~1 μm wide) at a fixed x-coordinate (and variable y) in the sample plane is dispersed to create a spectral image (y, λ, I_f). A series of such images was taken at different x coordinates (x-scanning), by moving the sample position in the x direction using a nano-positioning stage (MadCity-Labs, Nano-LP 100). Combination of this series in ImageJ [18] software allowed us to construct the hyperspectral cube. Andor Solis software was used to simultaneously control camera acquisition and spectrograph parameters. Typical excitation power at the sample plane for topographic, SPT, and spectral emission images were 0.50, 1.63, and 0.06 W cm^{-2} at 458 nm respectively, unless otherwise noted. Typical image pixel size was 360 nm. Diffraction limited size of individual emitting spots was confirmed using a 100x oil immersion objective lens (Motic, 1.25 NA) resulting in an image pixel size of 150 nm. Pixel sizes were calibrated using a grid distortion target (Thorlabs, R1L3S3P). For the acquisition images NP suspensions (~1.2×10^{-3} mg L^{-1}) were spincoated on freshly cleaned cover-slips to an average surface concentration <0.1 particle μm^{-2} to allow for individual particle identification. Diffraction-limited spots observed in the images were attributed to single particles because the number of spots varies linearly with the concentration of the suspensions used for spincoating. Cover-slips (Ted Pella Inc., Goldseal No. 1.5) were cleaned by immersion/sonication for 15 min in acetone, 15 min in water, and 1 h in H_2SO_4:H_2O_2 (1:4 v/v), followed by rinsing with abundant water and storing on MeOH. Right before use, cover-slips were retrieved from MeOH and flamed with a Bunsen burner to quickly eliminate the solvent.

The time dependence of fluorescence intensity of individual particles ($I_{f\text{-}SP}$) was determined from a time series of emission micrographs (microscope movies) recorded at 57.3 Hz for a total of 1000 frames and analyzed with home-written software. Excitation power at the sample plane was 18.7 W cm^{-2} at 488 nm.

Brownian motion analysis of single particle trajectory (BM-SPT)

Trajectories of individual freely diffusing particles in water were constructed from temporal series of fluorescence images (movies) acquired using the previously described microscope. The trajectories were later analyzed to characterize Brownian motion parameters and obtain single particle hydrodynamic radii distributions (*vide infra*). Samples were prepared by loading NP water suspensions (1.2×10^{-3} mg l^{-1}) in sealed chambers formed by placing a piece of double sided tape, having a central 5 mm circular hole, between two clean cover-slips (see figure S1 in the supplementary data, available at stacks.iop.org/MAF/5/024001/mmedia). The use of sealed chambers prevents the formation of convection currents in the sample that would invalidate the assumption of pure Brownian motion on the analyzed particles. Also, to minimize the detection of particles interacting with surfaces (hence not freely diffusing) data were acquired with the detection focal plane centered between the top and bottom cover-slip planes of the sample chamber. The distance between cover-slip planes was measured to be ~100 μm, while the depth of field of the instrument was measured to be < 2 μm (in excellent agreement with theoretical calculations [19]). This assures that the detected particles are relatively far from both top and bottom chamber surfaces. Movies were recorded at a frame rate of 31.23 Hz for a total of 500 frames and were later analyzed using the 'Mosaic Single-Particle Tracking Tool' routine [20] on ImageJ software to generate single particle trajectories and their corresponding mean diffusion coefficients (D). A detailed description of trajectory analysis, can be found in the supplementary data. The hydrodynamic diameter (d) for each particle/trajectory was calculated using D [21]:

$$d = \frac{k_b T}{3\pi\eta D} \quad (1)$$

where k_b is the Boltzmann constant, T the liquid's temperature (293 K), and η its viscosity (1 mPa s). More than 130 particles/trajectories were analyzed for each sample and used to construct the SPT hydrodynamic diameter distributions shown in figure 4. Sample movies used in these experiments are available for download in the supplementary data.

Absorption and emission spectroscopy

UV–vis absorption spectra were recorded on a diode-array spectrophotometer (Agilent Hewlett-Packard, HP 8452A) in 1 cm cuvettes at room temperature. Emission measurements were acquired from dilute solutions ($Abs_{max} < 0.1$) in 1 cm cuvettes at room temperature and with excitation at the sample absorption maximum. Emission spectra were recorded with a spectrofluorometer (Horiba, Fluoromax-4) using the following parameters: 1 nm slits for both the excitation and emission monochromators, 0.1 s integration time per point, and with automatic correction for the spectral instrument response.

Results and discussion

Nanoparticle size characterization

UV–visible absorption spectroscopy

Figures 1(a) and (b) show photographs and schematic representations of F8BT NP and F8BT@pEGDMA NP suspended in water. An increase in turbidity is observed in the F8BT@pEGDMA NP sample which suggests increased particle size compared to that of the

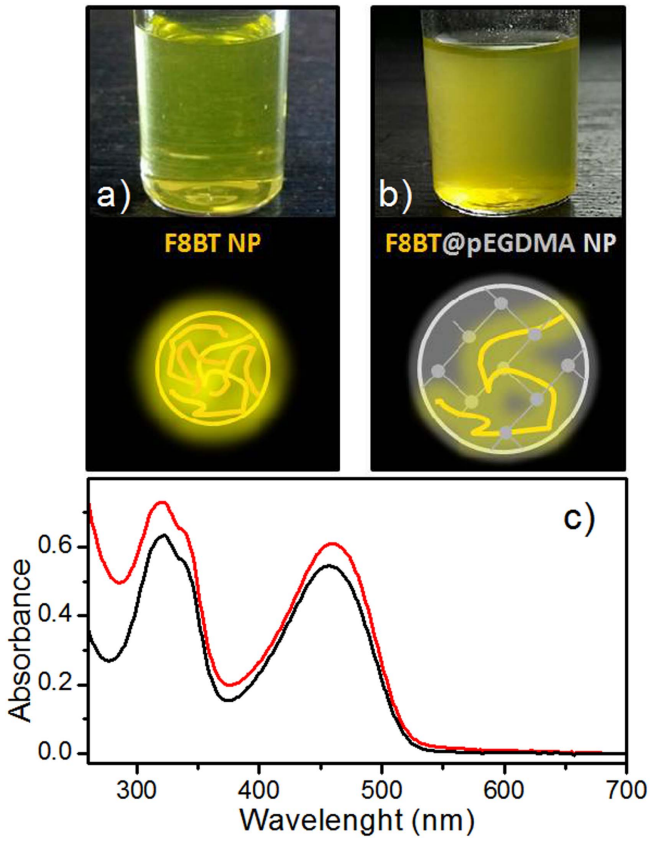

Figure 1. Photographs and schematic representation of F8BT NP (12 mg L^{-1}) (a) and F8BT@pEGDMA NP (12 mg L^{-1}) (b) suspended in water. (c) Absorption spectra of water suspensions of F8BT NP (black line) and F8BT@pEGDMA NP (red line).

F8BT NP sample. Figure 1(c) shows the absorption spectra of both F8BT (black line) and F8BT@pEGDMA NP (red line) suspensions in water. No significant differences are observed in the F8BT spectral bands of both samples, suggesting that the average conformation and composition of F8BT chains are not significantly affected by the crosslinking/polymerization of EGDMA monomers nor by the presence of KPS polymer initiator radicals. A slight increase in scattering is observed for F8BT@pEGDMA NP relative to F8BT NP, which is assigned to a particle size increase in the former.

AFM

Water suspensions of NP were deposited over clean mica substrates as described in the experimental section and particle heights were measured using AFM. Figures 2(a) and (b) show AFM images of F8BT NP and F8BT@pEGDMA NP samples. Figure 2(a) inset shows the size distribution of the F8BT NP with a mean height of 6 nm. Figure 2(b) inset shows a topographic profile corresponding to the white line in the image. In this case a particle size distribution was not constructed because most particles agglomerate during deposition. However the height of the agglomerates is less than 50 nm suggesting that individual particle sizes are smaller than this value.

DLS

Figure 3 shows hydrodynamic diameter distributions measured by DLS of F8BT NP (a) and F8BT@pEGDMA NP (b) suspended in water having a mean hydrodynamic diameter of 45 nm and 74 nm, respectively. The data confirm that the size of the F8BT@pEGDMA NP increases as compared to that of F8BT NP. The results are consistent with F8BT molecules being contained within larger crosslinked poly-EGDMA NP. The lack of agreement between AFM and DLS results for F8BT NP can be rationalized considering that particle height measured over mica surfaces might not be equivalent to its diameter due to potential deformations induced by particle–mica interactions. Additionally cantilever induced NP deformation can also affect the NP height histograms measured by AFM, although by using tapping mode the deformation is expected to be minimized [22]. Furthermore the large differences between AFM and DLS (or BM-SPT, *vide infra*) might be a partial consequence of particle aggregation in solution. Additionally hydrodynamic diameters are usually larger than particle heights measured in dry conditions due to particle solvation shell and particle shape deviations from perfect spherical symmetry assumed in the former [23].

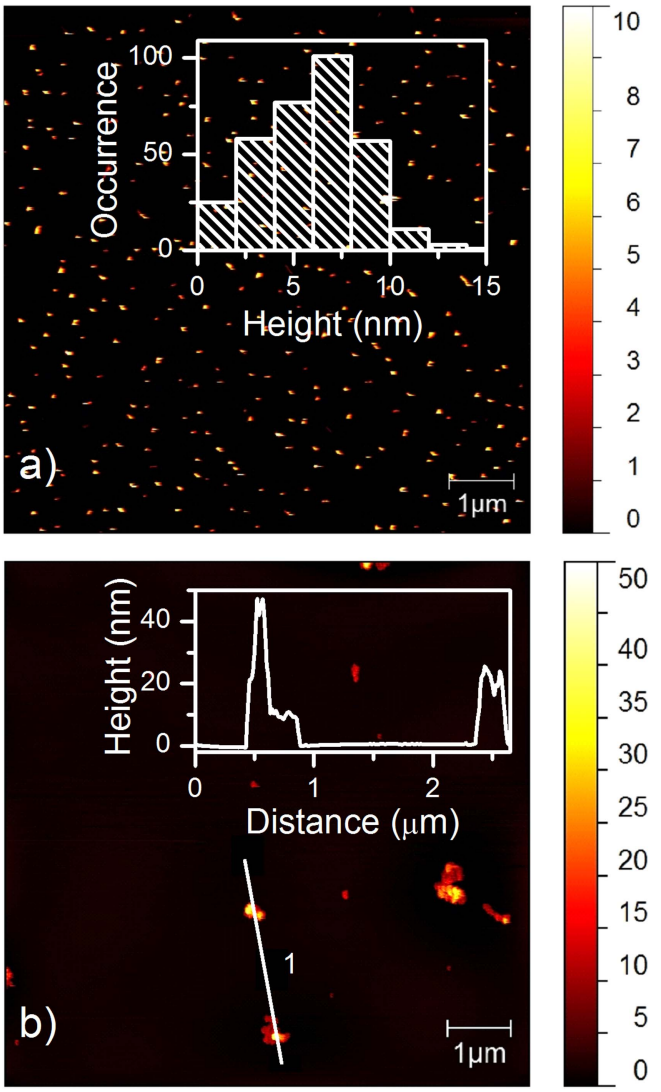

Figure 2. AFM images of F8BT NP (a) and F8BT@pEGDMA NP (b) over mica. False color height scale on the right is in nm. Inset panel (a): F8BT NP height distribution measured by AFM. Inset panel (b): topographic profile of line (1) shown in (b).

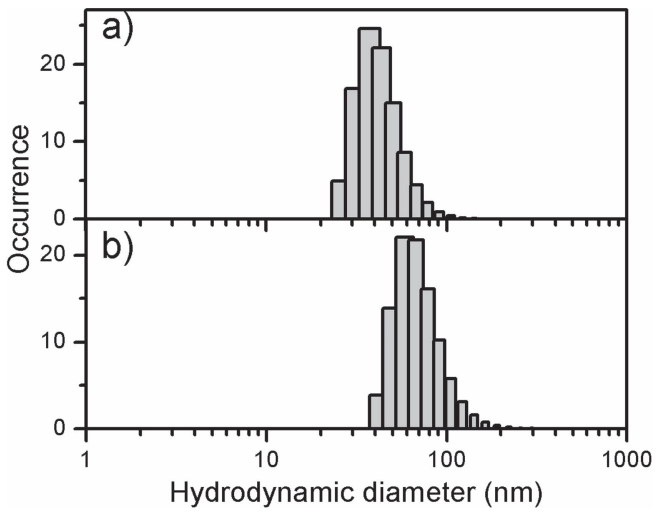

Figure 3. Hydrodynamic diameter histograms obtained by DLS of water suspensions of F8BT NP (a) and F8BT@pEGDMA NP (b).

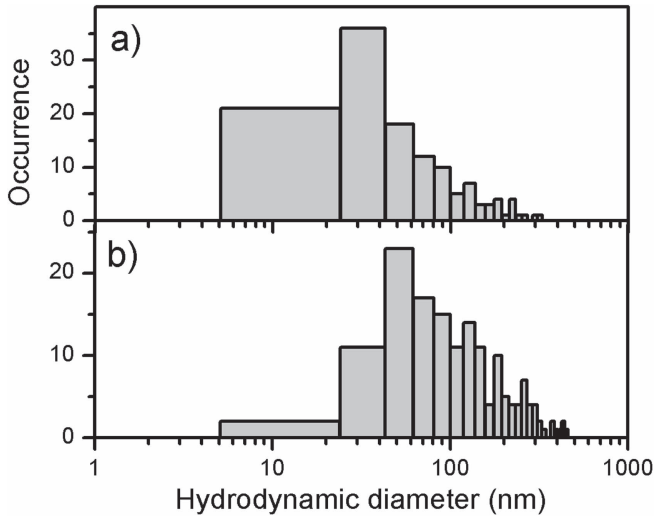

Figure 4. Hydrodynamic diameter histograms obtained through BM-SPT (see text for details) of water suspensions of F8BT NP (a) and F8BT@pEGDMA NP (b).

Table 1. NP size characterization results.

	Tech./measurement (nm)		
Sample NP	AFM[a]	DLS[b]	BM-SPT[b]
F8BT	6 (2.6)	45 (13)	75 (66)
F8BT@pEGDMA	<50[c]	74 (26)	142 (98)

[a] mean particle height,

[b] mean hydrodynamic diameter. Standard deviations are shown in parentheses.

[c] no distributions were recorded for this sample, see text.

BM-SPT

Analysis of individual particle trajectories, as described in the experimental section, for F8BT NP and F8BT@pEGDMA NP suspended in water, yielded hydrodynamic diameter distributions shown in figures 4(a) and (b), respectively. The mean hydrodynamic diameters obtained by this method, 120 nm for F8BT NP and 196 nm for F8BT@pEGDMA NP, show the same trend observed in DLS results. BM-SPT histograms provide real single-particle statistics and thus are, in principle, more representative of the true hydrodynamic diameter distribution than DLS histograms, which are constructed by fitting ensemble-averaged photon scattering autocorrelation functions. However the limited dynamic range imposed by the experimental conditions in BM-SPT hinders the detection of dim/small NP, biasing the size distribution towards brighter/larger NP. This effect could explain the differences observed in the hydrodynamic diameter distributions measured by DLS and BM-SPT. Size characterizations results are summarized in table 1.

Nanoparticle integrity characterization

Fluorescence microscopy

Figures 5(a) and (b) show fluorescence microscopy images of samples prepared by deposition of F8BT@pEGDMA NP suspensions in water and EtOAc respectively, on clean glass cover-slip substrates through spincasting. Diffraction limited bright emission spots observed in both images are assigned to fluorescence emission from individual NP.

The previous results confirm that the synthesis method allows us to obtain particles with nanometric dimensions that can be detected at the single particle level using fluorescence spectroscopy. The sample prepared from ethyl acetate (figure 5(b)) shows a clear increase of average background intensity compared to that prepared from water (figure 5(a)). At this point it is important to note that F8BT is soluble in EtOAc at low concentrations ($<10\,\mathrm{mg\,l^{-1}}$). Control experiments with samples prepared by depositing pure EtOAc over clean glass cover-slips (not shown) indicate that the background intensity observed in figure 5(b) is not due to fluorescent impurities present in EtOAc. These observations suggest that the relatively high background signal observed in figure 5(a) is due to individual F8BT chains that were not efficiently entrapped inside the crosslinked matrix of a fraction of F8BT@pEGDMA NP. Therefore F8BT chains were easily removed from this fraction of particles upon contact with EtOAc. On the other hand, the large number of intense emission spots observed in the sample deposited from EtOAc indicates that in a significant fraction of F8BT@pEGDMA NP, F8BT chains are efficiently retained. Thus in this latter fraction of particles the crosslinking/polymerization process was successful in maintaining the structural integrity after suspension in EtOAc.

To further test the integrity of F8BT@pEGDMA NP upon exposition to organic solvents, we performed

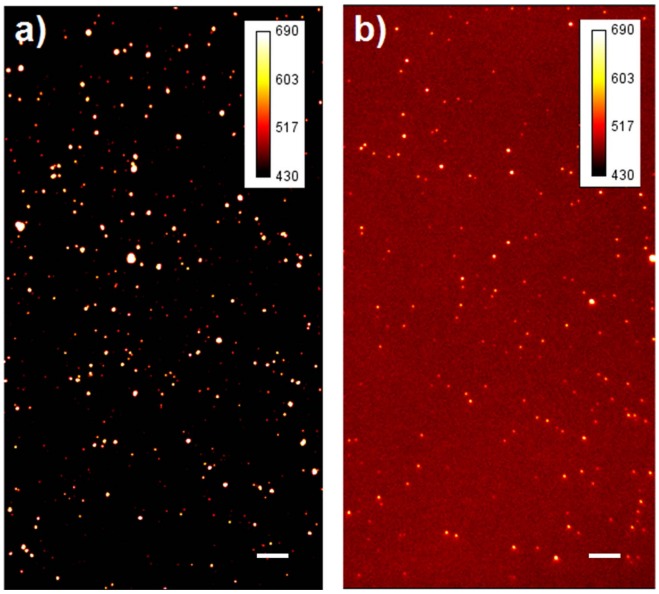

Figure 5. Emission micrograph of F8BT@pEGDMA NP deposited on clean cover-slip from water (a) and EtOAc (b) suspensions. Scale bar: 10 μm. I_f shown in false color scale.

the following comparative washing/dissolution experiment. Samples of F8BT NP and F8BT@pEGDMA NP were prepared by depositing water suspensions of the particles over clean cover-slips. Figures 6(a) and (b) show representative emission micrographs of samples containing F8BT NP and F8BT@pEGDMA NP, respectively. After initial imaging each sample was gently washed with toluene (good F8BT solvent) by carefully covering the whole cover-slip surface with solvent and then trickling the liquid by slowly turning the cover-slip vertically and letting it dry out. Figures 6(c) and (d) show representative emission micrographs of F8BT NP and F8BT@pEGDMA NP samples after washing. Statistical analysis (performed in several sample regions with ~500 particles/'field of view' before washing) indicates that 92% and 11% of particles are lost after the washing process, for F8BT NP and F8BT@pEGDMA NP samples, respectively. These results can be rationalized considering that in the F8BT NP sample the washing procedure leads to dissolution of most deposited particles due to the excellent solubility of F8BT in toluene (solubility $> 1\,\mathrm{g\,L^{-1}}$). On the other hand, the cross-linked pEGDMA matrix is not dissolved by toluene and might act as a retaining net hindering dissolution and removal of the entrapped F8BT chains. Thus it is likely that most of these particles maintain their integrity and remain adsorbed on the cover-slip after washing with toluene although other factors can also be at play.

Spectral fluorescence microscopy

To unequivocally elucidate the origin of background differences observed in cover-slip-deposited samples of F8BT@pEGDMA NP from water and EtOAc suspensions (as previously seen in figures 5(a) and (b)) we acquired hyperspectral data cubes for each sample. Figures 7(a) and (b) show the wavelength integrated (x, y, I_f) images of samples prepared by deposition of F8BT@pEGDMA NP from water and EtOAc, respectively. Figure 7(c) shows the emission spectra of two representative single F8BT@pEGDMA NP (green and red lines) marked with color coded arrows in figures 7(a) and (b), and the bulk corrected emission spectrum of F8BT NP in water suspension (black line). All spectra show almost identical features associated with F8BT emission, minor differences observed are associated with lack of correction, by microscope spectral response, on the single molecule spectra. These results are consistent with those of absorption spectra (figure 1) indicating that F8BT structure and conformation are not significantly altered by EGDMA crosslinking/polymerization. Figure 7(d) shows the average emission spectra from background regions in figures 7(a) (green line) and (b) (red line). Background regions were carefully selected to avoid the presence of individual particles. Both spectra were corrected by subtracting the background emission of a clean cover-glass under identical experimental conditions. The average spectrum from background regions in figure 7(b) (red line) shows characteristic features of F8BT emission, confirming that the relatively high background signal observed in samples of F8BT@pEGDMA NP deposited from EtOAc (figure 5(b)) is mainly due to free F8BT chains extracted from the particles by interaction with the solvent.

Single-particle fluorescence intensity fluctuations

Temporal fluorescence intensity fluctuations of individual particles were studied for F8BT@pEGDMA NP

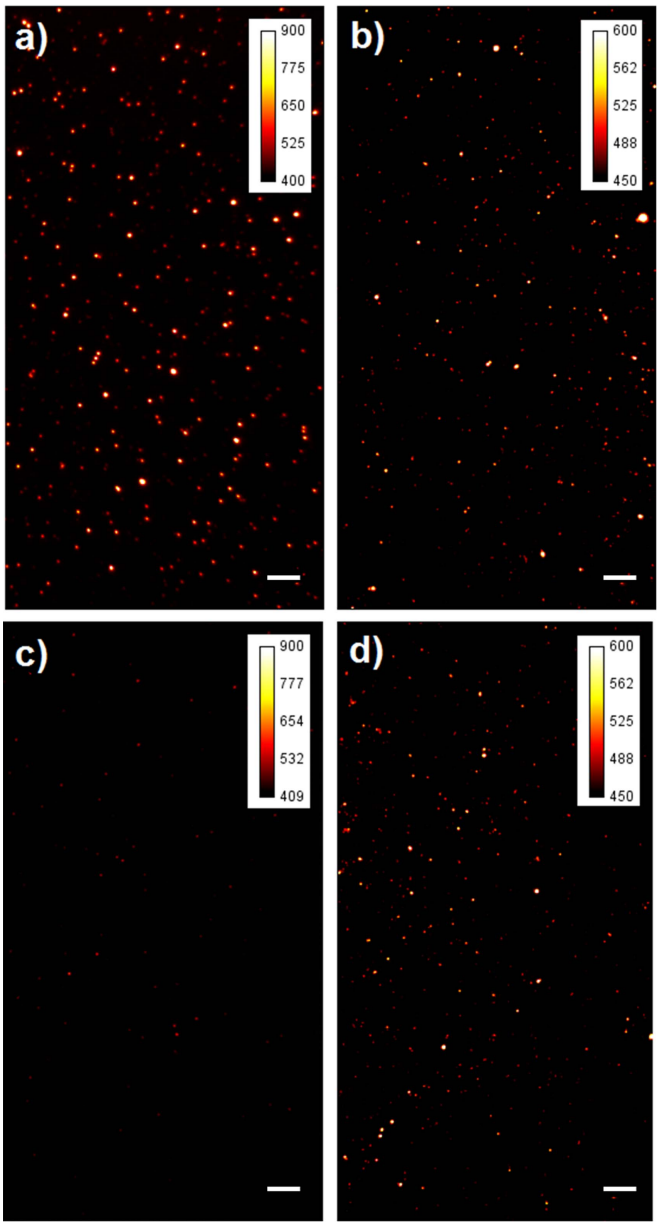

Figure 6. Representative fluorescence microscopy images of samples of F8BT NP (left column, (a) and (c)) and F8BT@pEGDMA NP (right column, (b) and (d)) deposited over glass cover-slips before (top row, (a) and (b)) and after (bottom row, (c) and (d)) toluene washing. Scale bar: 10 μm. Insets: I_f shown in false color scale.

and F8BT NP to gain deeper insight on their photophysical properties. Hundreds of individual-particle fluorescence-intensity transients were analyzed for each sample. For F8BT@pEGDMA NP samples ~52% of the particles show single step 'high/low' intensity fluctuations (blinking) whereas for F8BT NP samples less than 2% of the particles display such behavior.

Figures 8(a) and (c) show representative single-particle I_f transients displaying blinking behavior for F8BT@pEGDMA NP and F8BT NP, respectively. Sample movies used in these experiments are available for download in the supplementary data. Blinking in CP is known to be a consequence of efficient energy transfer among a large number of chromophores present in a single polymer chain. Due to this efficient transfer almost all excitation energy collected by the chain is funneled towards one (or a few) low-energy chromophore(s) that is(are) responsible for most I_f of that polymer molecule. When the excited state of the low-energy accepting chromophores are deactivated by a quencher, the I_f of the molecule is significantly reduced [24–29]. In contrast, CPNPs are usually comprised of several polymer chains and have a significantly larger number of chromophores as compared to single polymer molecules. In most CPNPs a considerable number of chromophores are responsible for the observed emission of individual particles, thus typically they do not display blinking behavior [30]. However some small CPNPs (aggregates comprised of 2–3 polymer chains) can also show blinking behavior. Figures 8(b) and (d) show representative single-particle I_f transients displaying non-

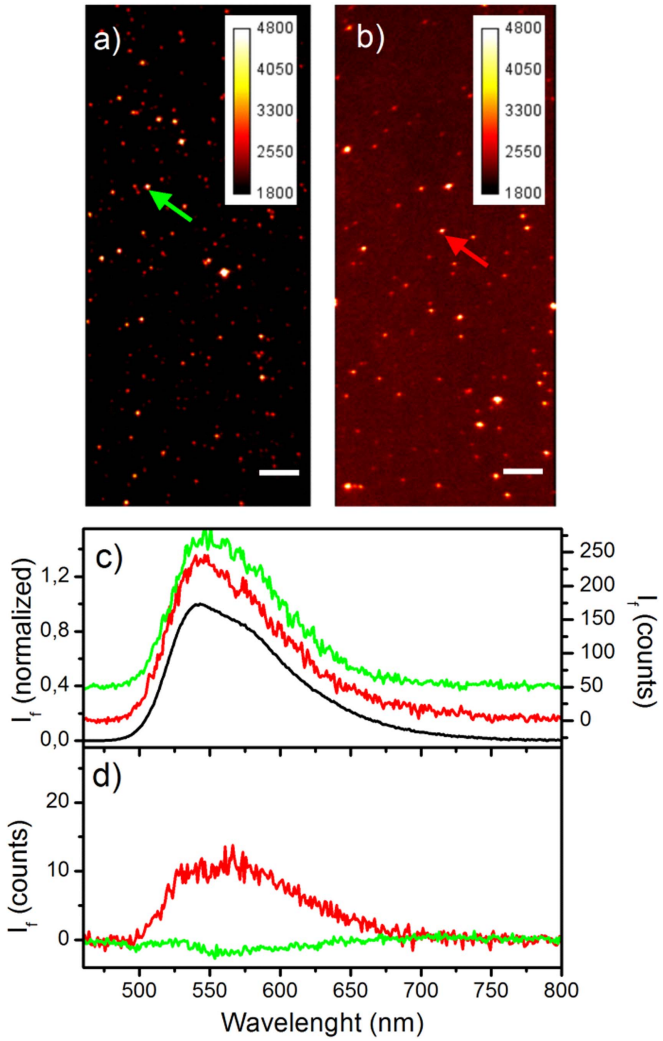

Figure 7. Emission micrographs of F8BT@pEGDMA NP (deposited over a clean cover-slide) from water (a) and EtOAc (b) suspensions. Scale bar: 10 μm. Inset: I_f in false color scale. (c) Single particle emission spectra of representative particles marked with an arrow in the upper panels (red and green color coded, right I_f scale) and ensemble emission spectrum of F8BT NP water suspension (black line, left I_f scale). Single particle spectra were offset to improve presentation. (d) Average emission spectra of background regions from panels (a) (green) and (b) (red).

blinking behavior for F8BT@pEGDMA NP and F8BT NP, respectively. Transients showing blinking on both samples are assigned to particles containing a single (or very few) F8BT chain(s) per particle (see figure 1(b) schematic representation). The relatively long 'low intensity' periods (>15 ms) observed in these I_f blinking transients (see figures 8(a) and (c)) are tentatively assigned to quenching by (reversibly formed) polymer/molecular-oxygen (O_2) adducts with charge transfer character ($polymer^{+}/O_2^{-}$) as previously reported for single molecules of an analogous CP [24]. These quenchers could form by reaction of O_2 with excited chromophores and disappear by back electron transfer. Electron deficiencies (such as radical-cations or hole-polarons) have been shown to be effective quenchers of excited chromophores in F8BT [5, 31, 32]. The blinking behavior of our F8BT@pEGDMA NP is particularly relevant for their application in ultrasensitive analyte detection schemes. In principle, the interaction of one of these particles with a single analyte molecule (acting as emission quencher) could lead to significant deactivation of its I_f thus providing a readily accessible analytical signal with single-molecule sensitivity. Figures 8(a) and (c) insets show single-particle I_f distributions and mean I_f ($\langle I_f \rangle$) of F8BT@pEGDMA NP and F8BT NP samples, respectively. The lower $\langle I_f \rangle$ and the larger fraction of blinking particles in the F8BT@pEGDMA NP sample are consistent with the interpretation that most of these particles contain a very small number of F8BT chains (in many cases only one) as compared to F8BT NP which contain a larger number of emitting polymer chains per particle, larger $\langle I_f \rangle$, and show almost no blinking.

Conclusions

F8BT@pEGDMA NP were successfully synthesized and characterized using an array of techniques, in

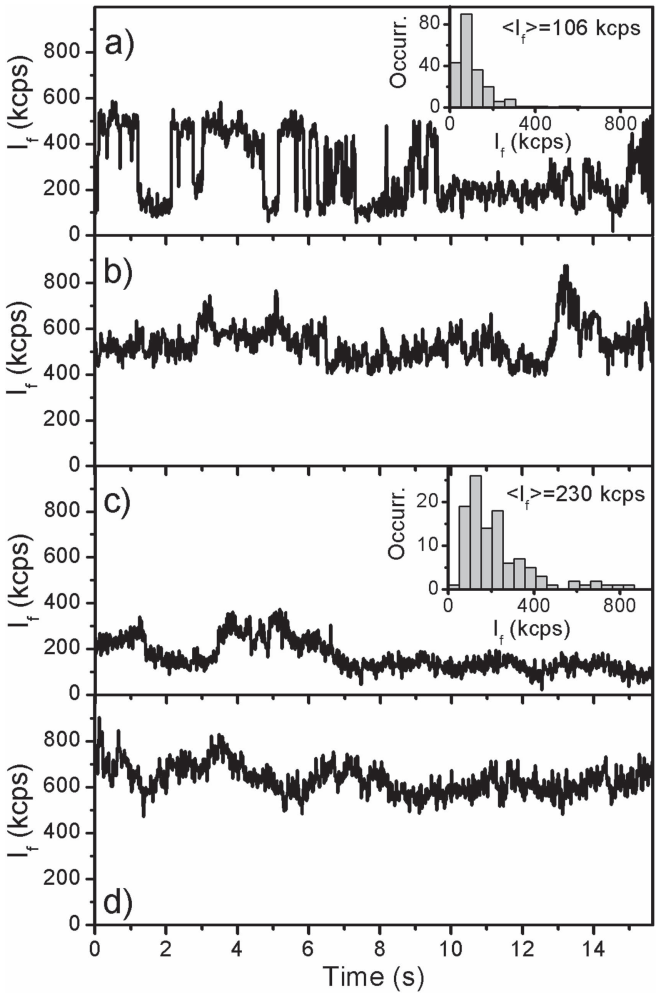

Figure 8. Representative single particle emission intensity transients of F8BT@pEGDMA NP ((a), (b)) and F8BT NP ((c), (d)) samples showing typical blinking ((a), (c)) and non-blinking ((b), (d)) behavior. Insets: single-particle fluorescence-intensity distributions of F8BT@pEGDMA NP (a) and F8BT NP (c) samples.

particular single particle fluorescence microscopy. The nanometric size of the prepared NP is adequate for high spatial-resolution sensing applications. The spectral properties of the conjugated polymer chains are not significantly affected by the crosslinking/polymerization process. Furthermore, fluorescence microscopy and spectral fluorescence microscopy observations demonstrate that most particles maintain their integrity upon contact with solvents that usually dissolve non-polar non-crosslinked polymers (e.g. EtOAc and toluene). This result indicates that the particles can withstand organic-solvent washing steps used in the preparation of MIP materials. Additionally we demonstrated that the emission of the newly developed particles can be monitored at the individual particle level with high spatial and temporal resolution using fluorescence microscopy. Moreover, it was found that a large fraction of F8BT@pEGDMA particles display fluorescence blinking characteristic of single conjugated polymer molecules, a behavior that is useful in sensing applications based in fluorescence super-quenching [33, 34]. These combined characteristics bode well for the use of F8BT@pEGDMA NP as MIP matrices for highly sensitive and selective analyte detection strategies. For example, several MIP NP systems capable of detecting specific analytes via luminescence transduction mechanisms have been reported in a recent review [35]. Furthermore, fluorescence sensing strategies in crosslinked conjugated polymer materials have been reported for detection of nitroaromatic compounds [12]. Finally our crosslinked-NP preparation strategy does not require complicated synthetic/purification procedures and, in principle, it is sufficiently flexible to allow for the incorporation of different commercially available CP into pEGDMA NP.

Acknowledgments

Authors acknowledge financial support of this work by grants from ANPCyT, Argentina (PICT 214/14); CONICET, Argentina (PIP 11220150100295CO/2015) and Secretaría de Ciencia y Técnica (SECyT), UNRC (PPI 2016) Argentina. The funders had no role in study design, data collection and analysis, decision

to publish, or preparation of the manuscript. MLG, CAC and REP are permanent research staff of CONICET. RAP and CVW thank CONICET for PhD and postdoctoral scholarships, respectively. YLM thanks SECyT UNRC for an undergraduate research scholarship.

Competing interests

The authors declare that no competing interests exist.

References

[1] Günes S, Neugebauer H and Sariciftci N S 2007 Conjugated polymer-based organic solar cells *Chem. Rev.* **107** 1324–38
[2] Coakley K M and McGehee M D 2004 Conjugated polymer photovoltaic cells *Chem. Mater.* **16** 4533–42
[3] Yamada T and Tsubata Y 2012 Recent progress and future perspectives of light emitting polymers for full-color display *J. Synth. Org. Chem. Jpn.* **70** 473–9
[4] Rahman M A, Kumar P, Park D-S and Shim Y-B 2008 Electrochemical sensors based on organic conjugated polymers *Sensors* **8** 118–41
[5] Palacios R E, Fan F-R F, Grey J K, Suk J, Bard A J and Barbara P F 2007 Charging and discharging of single conjugated-polymer nanoparticles *Nat. Mater.* **6** 680–5
[6] Chang Y-L, Palacios R E, Fan F-R F, Bard A J and Barbara P F 2008 Electrogenerated chemiluminescence of single conjugated polymer nanoparticles *J. Am. Chem. Soc.* **130** 8906–7
[7] Palacios R E, Chang W-S, Grey J K, Chang Y-L, Miller W L, Lu C-Y, Henkelman G, Zepeda D, Ferraris J and Barbara P F 2009 Detailed single-molecule spectroelectrochemical studies of the oxidation of conjugated polymers *J. Phys. Chem.* B **113** 14619–28
[8] Palacios R E, Lee K-J, Rival A, Adachi T, Bolinger J C, Fradkin L and Barbara P F 2009 Single conjugated polymer nanoparticle capacitors *Chem. Phys.* **357** 21–7
[9] Haupt K 2003 Imprinted polymers—tailor-made mimics of antibodies and receptors *Chem. Commun.* 171–8
[10] Torres J J, Montejano H A and Chesta C A 2012 Characterization of imprinted microbeads synthesized via minisuspension polymerization *Macromol. Mater. Eng.* **297** 342–52
[11] Komiyama M, Takeuchi T and Mukawa T 2003 *Molecular Imprinting: From Fundamentals to Applications* (Weinheim: Wiley)
[12] Li J, Kendig C E and Nesterov E E 2007 Chemosensory performance of molecularly imprinted fluorescent conjugated polymer materials *J. Am. Chem. Soc.* **129** 15911–8
[13] Hunkeler D 1991 Mechanism and kinetics of the persulfate-initiated polymerization of acrylamide *Macromolecules* **24** 2160–71
[14] Pérez N, Whitcombe M J and Vulfson E N 2000 Molecularly imprinted nanoparticles prepared by core–shell emulsion polymerization *J. Appl. Polym. Sci.* **77** 1851–9
[15] Fonseca T, Relógio P, Martinho J M G and Farinha J P S 2007 Preparation and surface characterization of polymer nanoparticles designed for incorporation into hybrid materials *Langmuir* **23** 5727–34
[16] Garay-Jimenez J C, Young A, Gergeres D, Greenhalgh K and Turos E 2008 Methods for purifying and detoxifying sodium dodecyl sulfate–stabilized polyacrylate nanoparticles *Nanomedicine Nanotechnol. Biol. Med.* **4** 98–105
[17] Nečas D and Klapetek P 2012 Gwyddion: an open-source software for SPM data analysis *Open Phys.* **10** 181–8
[18] Schneider C A, Rasband W S and Eliceiri K W 2012 NIH Image to ImageJ: 25 years of image analysis *Nat. Methods* **9** 671–5
[19] Shillaber C P 1944 *Photomicrography: In Theory and Practice* (London: Chapman & Hall)
[20] Sbalzarini I F and Koumoutsakos P 2005 Feature point tracking and trajectory analysis for video imaging in cell biology *J. Struct. Biol.* **151** 182–95
[21] Atkins P W and De Paula J 2006 *Atkins' Physical Chemistry* (New York: Freeman)
[22] Zhang H, Honda Y and Takeoka S 2013 Tapping-mode AFM study of tip-induced polymer deformation under geometrical confinement *Langmuir* **29** 1333–9
[23] Baalousha M and Lead J R 2012 Rationalizing nanomaterial sizes measured by atomic force microscopy, flow field-flow fractionation, and dynamic light scattering: sample preparation, polydispersity, and particle structure *Environ. Sci. Technol.* **46** 6134–42
[24] Yu J, Hu D and Barbara P F 2000 Unmasking electronic energy transfer of conjugated polymers by suppression of O_2 quenching *Science* **289** 1327–30
[25] Huser T, Yan M and Rothberg L J 2000 Single chain spectroscopy of conformational dependence of conjugated polymer photophysics *Proc. Natl Acad. Sci. USA* **97** 11187–91
[26] Bolinger J C, Traub M C, Adachi T and Barbara P F 2011 Ultralong-range polaron-induced quenching of excitons in isolated conjugated polymers *Science* **331** 565–7
[27] Lin H, Tabaei S R, Thomsson D, Mirzov O, Larsson P-O and Scheblykin I G 2008 Fluorescence blinking, exciton dynamics, and energy transfer domains in single conjugated polymer chains *J. Am. Chem. Soc.* **130** 7042–51
[28] Vogelsang J, Adachi T, Brazard J, Vanden Bout D A and Barbara P F 2011 Self-assembly of highly ordered conjugated polymer aggregates with long-range energy transfer *Nat. Mater.* **10** 942–6
[29] Dalgarno P A, Traina C A, Penedo J C, Bazan G C and Samuel I D W 2013 Solution-based single molecule imaging of surface-immobilized conjugated polymers *J. Am. Chem. Soc.* **135** 7187–93
[30] Grey J K, Kim D Y, Norris B C, Miller W L and Barbara P F 2006 Size-dependent spectroscopic properties of conjugated polymer nanoparticles *J. Phys. Chem.* B **110** 25568–72
[31] Palacios R E, Fan F-R F, Bard A J and Barbara P F 2006 Single-molecule spectroelectrochemistry (SMS-EC) *J. Am. Chem. Soc.* **128** 9028–9
[32] Bolinger J, Lee K-J, Palacios R E and Barbara P F 2008 Detailed investigation of light induced charge injection into a single conjugated polymer chain *J. Phys. Chem.* C **112** 18608–15
[33] Swager T M 1998 The molecular wire approach to sensory signal amplification *Acc. Chem. Res.* **31** 201–7
[34] Chen L, McBranch D W, Wang H-L, Helgeson R, Wudl F and Whitten D G 1999 Highly sensitive biological and chemical sensors based on reversible fluorescence quenching in a conjugated polymer *Proc. Natl Acad. Sci. USA* **96** 12287–92
[35] Wackerlig J and Lieberzeit P A 2015 Molecularly imprinted polymer nanoparticles in chemical sensing—synthesis, characterisation and application *Sensors Actuators* B **207** 144–57